

Beyond Fixed Variables: Expanding-variate Time Series Forecasting via Flat Scheme and Spatio-temporal Focal Learning

Minbo Ma

School of Computing and Artificial Intelligence
Southwest Jiaotong University
Chengdu, China
minboma@my.swjtu.edu.cn

Kai Tang

School of Computing and Artificial Intelligence
Southwest Jiaotong University
Chengdu, China
tangkailh@outlook.com

Huan Li

School of Data Science and Engineering
Zhejiang University
Hangzhou, China
lihuan.cs@zju.edu.cn

Fei Teng

School of Computing and Artificial Intelligence
Southwest Jiaotong University
Chengdu, China
fteng@swjtu.edu.cn

Dalin Zhang

Hangzhou Dianzi University
Hangzhou, China
dalinzhang@ieee.org

Tianrui Li

School of Computing and Artificial Intelligence
Southwest Jiaotong University
Chengdu, China
trli@swjtu.edu.cn

ABSTRACT

Multivariate Time Series Forecasting (MTSF) has long been a key research focus. Traditionally, these studies assume a fixed number of variables, but in real-world applications, Cyber-Physical Systems often expand as new sensors are deployed, increasing variables in MTSF. In light of this, we introduce a novel task, *Expanding-variate Time Series Forecasting* (EVTSF). This task presents unique challenges, specifically (1) handling inconsistent data shapes caused by adding new variables, and (2) addressing imbalanced spatio-temporal learning, where expanding variables have limited observed data due to the necessity for timely operation. To address these challenges, we propose STEV, a flexible spatio-temporal forecasting framework. STEV includes a new *Flat Scheme* to tackle the inconsistent data shape issue, which extends the graph-based spatio-temporal modeling architecture into 1D space by flattening the 2D samples along the variable dimension, making the model variable-scale-agnostic while still preserving dynamic spatial correlations through a holistic graph. Additionally, we introduce a novel *Spatio-temporal Focal Learning* strategy that incorporates a negative filter to resolve potential conflicts between contrastive learning and graph representation, and a focal contrastive loss as its core to guide the framework to focus on optimizing the expanding variables. To evaluate the effectiveness of STEV, we benchmark EVTSTF performance on three real-world datasets from various domains and compare it against three potential solutions employing state-of-the-art (SOTA) MTSF models tailored for EVSTF. Experimental results show that STEV significantly outperforms its competitors, especially in handling expanding variables. Notably, STEV, with only 5% of observations during the expanding period, is on par with SOTA MTSF models trained with complete data. Further exploration of

various expanding scenarios underscores the generalizability of STEV in real-world applications.

KEYWORDS

Expanding-variate Time Series Forecasting, Spatio-temporal Graph Neural Networks, Contrastive Learning

1 INTRODUCTION

Multivariate Time Series (MTS), reflecting the fluctuation of multiple sensors' measurements over time, plays a vital role in understanding and optimizing Cyber-Physical Systems (CPS) across various domains [1, 31, 41]. As a fundamental task and a research hotspot in MTS utilization, MTS Forecasting (MTSF) necessitates a keen consideration of both the temporal dynamics of each variable and the spatial correlations across variables [13, 16, 36]. While recent advancements in MTSF have focused on developing novel deep learning networks to enhance forecasting accuracy, progress has nearly plateaued, often neglecting critical real-world requirements.

In this study, we instead draw attention to a frequently overlooked scenario in MTS research: *Expanding-variate Time Series* (EVT), where the number of variables dynamically increases over time. Specifically, we explore situations where an established CPS evolves with newly deployed sensors, which are expected to function with their supporting model as soon as possible. Consider a traffic management system, as illustrated in Fig. 1. Initially, sensors (black dots) monitor traffic conditions within a designated area (yellow shadow). As urban development progresses, additional sensors (red dots) are deployed, expanding the monitoring area (expanded yellow shadow). In this evolving context, we define the initially deployed sensors as *continual sensors*, and their measurements as *continual variables*, while the newly deployed sensors and their measurements are termed *expanding sensors* and *expanding variables*, respectively.

We will focus on the EVT Forecasting (EVTSTF) task, which aims to accurately forecast future values of both continual and expanding variables. In particular, the newly installed sensors are

Permission to make digital or hard copies of part or all of this work for personal or classroom use is granted without fee provided that copies are not made or distributed for profit or commercial advantage and that copies bear this notice and the full citation on the first page. Copyrights for third-party components of this work must be honored. For all other uses, contact the owner/author(s).

KDD '25, August 3–7, 2025, Toronto, ON, Canada

© 2025 Copyright held by the owner/author(s).

ACM ISBN XXXXXXXX-XXXXXXX.

<https://doi.org/XXXXXXX.XXXXXXX>

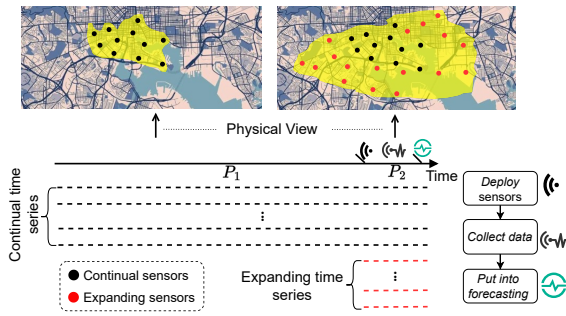


Figure 1: Expanding-variate Time Series in traffic monitoring. Left: Initial system with continual sensors (black dots) during period P_1 . Right: Expanded system with both continual and expanding sensors (black and red dots) during P_2 .

expected to perform forecasting upon deployment. Early forecasting is highly beneficial. For instance, in transportation, timely predictions of future traffic conditions in newly monitored regions can help reduce accidents during critical early stages. Similarly, in power systems, substantial ice accumulation on transmission lines can cause widespread power outages, as has been extensively documented in both China [8] and the United States [24]. To mitigate such risks, monitoring devices like tension sensors are deployed to detect ice buildup, where tension forecasting supports prompt deciding measures. In both scenarios, initiating forecasts immediately after sensor deployment is essential for effective risk prevention and mitigation.

Despite its many advantages, this task not only shares the common challenge of capturing spatio-temporal dependencies but also faces two additional major challenges:

- **Challenge 1: Inconsistent data shapes.** As new variables are introduced, the shape of the data changes, as shown in Fig. 1. This necessitates that deep model training adapts to varying dimensions within the same mini-batch, a stark contrast to the equal-sized data shapes assumed by traditional training methods. An intuitive strategy is to treat EVTS as a set of independent univariate times series (UTS) and perform forecasting for each UTS individually. However, this approach fails to leverage correlations among variables, limiting its effectiveness. Another strategy is to apply the padding operation to standardize sample shapes, but this often introduces noise, resulting in inevitably inferior performance (refer to the evaluation in Section 4.2). Besides, several studies [4, 29] employ continual learning [27], which sequentially updates models using newly available data. While this approach is feasible in dynamic settings, its effectiveness is constrained by the catastrophic forgetting problem [12], i.e., neural models significantly forget previously learned information upon learning new data.
- **Challenge 2: Imbalanced spatio-temporal learning.** Newly deployed sensors need to start providing accurate forecasts as soon as possible. However, collecting enough data to fully capture the new spatio-temporal patterns takes time. This leads to a significant imbalance in the volume of data available, with the long-term observations ($P_1 + P_2$ in Fig. 1) of continual variables

and only very short-term data (P_2 in Fig. 1) of expanding variables. As a result, models trained under these conditions are often biased toward the well-represented continual variables, resulting in less accurate predictions for the newly added expanding variables. Conventional methods focus on increasing samples of expanding variables through techniques like oversampling and data augmentation. However, these approaches can easily lead to overfitting, especially when the synthetic data fails to adequately represent the expanding variables. Besides, previous studies have employed large language model fine-tuning [42] and channel-independent approaches [19] to enhance models with few-shot learning capabilities, they face challenges in capturing sequential dependencies in time series and effectively modeling spatial dependencies [25].

To tackle these challenges, we propose STEV, a generic Spatio-Temporal neural forecasting framework for EVTSF. For **Challenge 1**, we introduce a simple yet effective *Flat Scheme* (FLATS), which flattens EVTS along the variable dimension, transforming it into UTS, thereby making the model variable scale-agnostic. To preserve the spatial correlations in the original EVTS, we then present a holistic graph where isolated subgraphs maintain these spatial relationships. For **Challenge 2**, Inspired by the success of contrastive learning (CL) in capturing powerful representations from limited data [3, 32, 38], we introduce *Spatio-temporal Focal Learning* (STFL) to guide the model in learning more effective representations for the undersampled expanding variables. Our approach begins with negative sample filtering, designed to resolve conflicts between the negative sample generation strategy and the spatial neighbouring similarities. Building on this, we then introduce *Focal Contrastive Learning* (FOCALCL), which incorporates a newly designed focal temperature factor into the contrastive learning loss, ensuring that the optimization process prioritizes expanding variables, thereby enhancing learning effectiveness. Extensive experiments on three real-world EVTS datasets confirm that STEV not only outperforms potential state-of-the-art (SOTA) solutions but also demonstrates robustness across various expanding scenarios. In summary, our contributions are fourfold:

- (1) We introduce an emerging task, EVTSF, addressing a frequently overlooked aspect of CPS, that is evolving with sensing expansion. In response, we present STEV, a pioneering framework designed to tackle the unique challenges of EVTSF. (Sections 2 & 3)
- (2) We develop FLATS, a solution to the challenge of inconsistent-shaped mini-batches specific to EVTSF. This straightforward yet effective method preserves original spatial correlations while transforming variable-shaped data into a consistent format. (Section 3.2)
- (3) To address the issue of imbalanced spatio-temporal learning, we propose STFL, an unsupervised auxiliary task that enhances the learning of spatio-temporal representations for the under-sampled expanding variables. (Section 3.3)
- (4) Our experiments involve creating three diverse EVTS datasets across various domains to evaluate the STEV framework. The results show that STEV delivers performance comparable to SOTA MTSF methods using complete data, even when leveraging only 5% of the observed data. (Section 4)

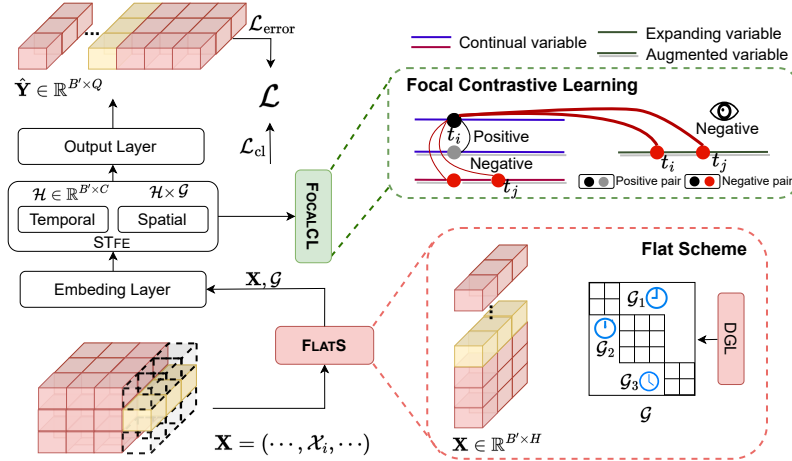


Figure 2: The overview of proposed framework STEV for EVTTSF. Given EVTTS data, STEV includes two components to overcome the inconsistent shape and imbalanced learning issues. Within the *Flat Scheme*, EVTTS data are flattened along the variable dimension. Meanwhile, DGL generates time-aware graph adjacency matrices. *Focal Contrastive Learning* aims to learn discriminative representations from outputs of spatio-temporal feature extractor (STFE), especially for expanding variables through focal contrastive loss. The joint loss combines the forecasting error loss and contrastive loss.

2 PROBLEM DEFINITION

We focus on defining the EVTTSF problem within an individual expansion process. Consecutive expansions can be treated as repeated instances of this process.

DEFINITION 1 (EXPANDING-VARIATE TIME SERIES). Let \mathcal{V}_1 and \mathcal{V}_2 denote the sets of variables before and after expansion, respectively. \mathcal{V}_1 includes only continual variables, while \mathcal{V}_2 encompasses both continual and expanding variables, thus $\mathcal{V}_1 \subset \mathcal{V}_2$. The EVTTS dataset \mathcal{D} consists of two main components: MTS data before variable expansion $\mathcal{D}_1 \in \mathbb{R}^{|\mathcal{V}_1| \times |P_1|}$ and after variable expansion $\mathcal{D}_2 \in \mathbb{R}^{|\mathcal{V}_2| \times |P_2|}$, i.e., $\mathcal{D} = (\mathcal{D}_1, \mathcal{D}_2)$. To ensure seamless forecasting upon new sensor installation, the observed time steps after expansion should be significantly fewer than those before expansion, i.e., $|P_2| \ll |P_1|$.

DEFINITION 2 (EXPANDING-VARIATE TIME SERIES FORECASTING). We aim to build an EVTTSF function \mathcal{F} that forecasts the future values for both continual and expanding variables. Formally,

$$\hat{\mathbf{Y}} = \mathcal{F}(\mathbf{X}), \quad (1)$$

where $\mathbf{X} \in \mathbb{R}^{|\mathcal{V}_2| \times H}$ represents the historical observations and $\hat{\mathbf{Y}} \in \mathbb{R}^{|\mathcal{V}_2| \times Q}$ represents the predictions, H and Q denote the historical and forecasting horizons, respectively.

PROBLEM (EXPANDING-VARIATE TIME SERIES FORECASTING). We define the data-driven optimization problem for $\mathcal{F}^*(\cdot)$ with the parameter θ as follows:

$$\mathcal{F}_\theta^* \leftarrow \underset{\mathcal{F}_\theta}{\operatorname{argmin}} \mathbb{E}_{\mathcal{X}_i, \mathcal{Y}_i \sim \mathcal{D}} [\mathcal{L}(\mathcal{F}_\theta(\mathcal{X}_i), \mathcal{Y}_i)], \quad (2)$$

where $\mathcal{X}_i \in \mathbb{R}^{N \times H}$, $\mathcal{Y}_i \in \mathbb{R}^{N \times Q}$ are drawn from \mathcal{D} using the sliding window technique, and $\mathcal{L}(\cdot)$ is the objective loss function. Notably, we mix and shuffle the data from before and after the variable expansion during the model optimization process. Therefore, the variable dimension N in Equation (2) equals to $|\mathcal{V}_1|$ if the samples are from before expansion, and $|\mathcal{V}_2|$ otherwise.

3 METHOD

3.1 Overview

Figure 2 provides an overview of STEV, highlighting two innovations integrated into general MTSF models: FLATS and FOCALCL. As discussed in Challenge 1, EVTTS data contains varying numbers of variables, whereas conventional methods generally handle regular tensors. To address this issue, we propose *FLATS* to flatten the EVTTS along the variable dimension, enabling a model to handle an arbitrary number of variables. We additionally present a *holistic isolated graph* to preserve the spatial correlations within variables, which are disordered when flattening. For each subgraph within the holistic isolated graph, we introduce the *dynamic graph learning* (DGL) scheme to adaptively represent the time-dependent spatial correlations. Addressing Challenge 2, we draw inspiration from contrastive learning’s ability to derive robust representations from limited labeled data. We propose *STFL* with a negative sample filter and a *FOCALCL* to derive robust and discriminative representations. These two custom mechanisms enable the model to avoid hard negative samples and focus on optimizing representations of expanding variables with limited observed data. The final optimization objective \mathcal{L} is a combination of traditional forecasting loss $\mathcal{L}_{\text{error}}$ and FOCALCL loss \mathcal{L}_{cl} .

3.2 Flat Scheme (FLATS)

The variable expansion causes inconsistencies in sample data shapes within a mini-batch, rendering traditional MTSF training methods that depend on uniform shapes ineffective for the EVTTSF task. One straightforward solution to this issue is the padding scheme, where samples are padded with constant values (e.g., zeros) to achieve uniformity, and a graph is to represent inter-variable correlations, as shown in the upper part of Figure 3. However, this approach inevitably introduces disturbances from the padding values, which persist despite applying a mask to the loss function to minimize their impact. To address this problem, we propose a simple yet effective

FLATS. As shown in the bottom part of Figure 3, we first transform 2D MTS data into 1D univariate time series (UTS) data and then employ a holistic isolated graph to retain the spatial correlations among the flat univariate time series.

3.2.1 Flat Transformation. Suppose we have a mini-batch EVTS samples $\mathbf{X} = \{\mathcal{X}_i\}_{i=1}^B$ (Figure 3 left), where B is the batch size and \mathcal{X}_i is an EVTS sample. $\mathcal{X}_i \in \mathbb{R}^{|\mathcal{V}_1| \times H}$ if it is before expansion and $\mathcal{X}_i \in \mathbb{R}^{|\mathcal{V}_2| \times H}$ if it is after expansion. To handle the inconsistent data shapes, we flatten \mathbf{X} along the variable dimension, transforming it into a new mini-batch $\mathbf{X}' = [\mathcal{X}'_i | i = 1, 2, \dots, B']$ (Figure 3 bottom), where $\mathcal{X}'_i \in \mathbb{R}^H$ is an UTS and $B' \in [B \times |\mathcal{V}_1|, B \times |\mathcal{V}_2|]$ represents the total count of samples in the mini-batch \mathbf{X}' . This flattening process converts the original batch \mathbf{X} with different-shaped MTS samples into a new batch \mathbf{X}' with uniform-shaped UTS samples, ensuring consistency in data shape for effective model training. However, this process loses the correlations among variables in the original samples. Therefore, we propose a holistic isolated graph to preserve the essential relationships between variables, enabling seamless spatial feature extraction.

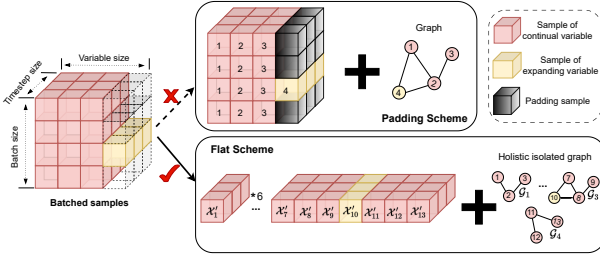


Figure 3: FLATS vs. padding scheme for EVTSF.

3.2.2 Holistic Isolated Graph. The original EVTS \mathbf{X} uses a graph structure to represent spatial correlations among variables. Inspired by the advanced mini-batching module of PyG [9], which efficiently handles multiple graphs with varying numbers of nodes by stacking them diagonally, we propose the holistic isolated graph to maintain these spatial correlations within the flattened samples.

In the original graph (Figure 3 top), each sample shares a uniform structure. Differently, the holistic isolated graph (Figure 3 bottom) comprises a disconnected collection of B distinct subgraphs $\{\mathcal{G}_i\}_{i=1}^B$, each corresponding to consecutive UTS samples in \mathbf{X}' , which align with their pre-expanding sample \mathcal{X}_i in \mathbf{X} . For instance, in the mini-batch in Figure 3, before flattening, the original graph represents the spatial correlations of the post-expansion sample that is \mathcal{X}_3 , containing variables 1 to 4. After flattening, samples \mathcal{X}'_7 to \mathcal{X}'_{10} correspond to the original sample \mathcal{X}_3 and share a subgraph \mathcal{G}_3 , while the other flat samples have their own subgraphs. This method not only ensures the spatial relationships are retained but also keeps a specific subgraph for each original sample.

Then we introduce the DGL module to construct the subgraph \mathcal{G}_i . Considering that in real-world CPS, pre-defined spatial correlations are not always available, we propose to construct learnable graph structures. In addition, the spatial correlations are not static but reveal periodic characteristics as time evolves due to regular production activities [18]. The adjacency matrix of the learnable

time-aware subgraph \mathcal{G}_i at time t is derived as follows:

$$\mathbf{A}_{t,i} = \text{SPARSE}(\mathbf{E}_t \cdot \mathbf{E}_i^T), \text{ where } \mathbf{E}_t = \text{CAT}(\mathbf{E}, e_t). \quad (3)$$

Here, $\mathbf{E} \in \mathbb{R}^{N \times d}$ represents the d -dimensional learnable embeddings of the N variables, and $e_t = \text{CAT}(e_{\text{tod}}, e_{\text{dow}})$ is a joint periodic embedding combining the time-of-day (tod) and the day-of-week (dow). The $\text{CAT}(\cdot, \cdot)$ operation concatenates these embeddings concatenation operation. The periodic embedding is also learnable during training and indexable during inference. The $\text{SPARSE}(\cdot)$ function applies a sigmoid activation followed by a filter operation that retains positive correlations, enhancing generalization while reducing computational overhead. This DGL scheme ensures that the spatial correlations within the subgraph \mathcal{G}_i are both adaptive and reflective of temporal periodicities.

3.3 Spatio-temporal Focal Learning (STFL)

After flattening the original mini-batch \mathbf{X} , we use a spatio-temporal feature extractor (STFE) to derive meaningful features. The STFE processes the flattened mini-batch \mathbf{X}' and the corresponding holistic isolated graphs $\{\mathcal{G}_i\}_{i=1}^B$, producing the output $\mathcal{H} = \text{STFE}(\mathbf{X}', \mathcal{G})$. Here, $\mathcal{H} \in \mathbb{R}^{B' \times C_{\text{out}}}$ with C_{out} representing the output dimension. This extractor employs a deep residual architecture comprising multiple blocks, each containing multi-layer 1D dilated convolutions [37] to capture temporal dynamics across different receptive fields, and Chebyshev spectral graph convolutions [7] to extract intricate spatial features. Detailed of the STFE can be found in Appendix A.1.

As indicated in **Challenge 2**, the issue of data imbalance tends to push the STFE towards focusing on continual variables with abundant data, resulting in insufficient representations of data-limited expanding variables. Traditionally, over-sampling and data augmentation are employed to address such imbalances by generating more samples for the minority class. However, merely increasing the number of minority samples does not necessarily enrich their semantic information and may lead to overfitting. Additionally, augmenting time series data poses a particular challenge, as it requires introducing diversity without corrupting the inherent temporal patterns. To circumvent these issues, we introduce a novel spatio-temporal focal learning approach. This method incorporates an innovative unsupervised FOCALCL mechanism with negative pair filtering, specifically designed to adapt to the FLATS and enhance the feature extraction for expanding variables.

3.3.1 Spatio-temporal Contrastive Learning. Vanilla contrastive learning aims to learn temporal representations and capture variable heterogeneity by pulling positive samples closer together and pushing negative samples apart. It has shown superiority in robust representation learning when only limited data is available [14, 38]. The core components of contrastive learning include the construction of positive and negative sample pairs and the contrastive loss.

Formally, to construct positive and negative sample pairs, a time series augmentation technique generates an additional view $\mathbf{X}'^{\text{aug}} \sim p(\mathbf{X}'^{\text{aug}} | \mathbf{X})$. The augmentation conditional distribution $p(\cdot | \mathbf{X})$ reflects the transformational impact of augmentation techniques on the temporal dynamics of the time series. A sample and its augmented counterpart are treated as a positive pair, i.e., $(\mathcal{X}'_i, \mathcal{X}'_i^{\text{aug}})$, while the sample and the augmented counterparts of

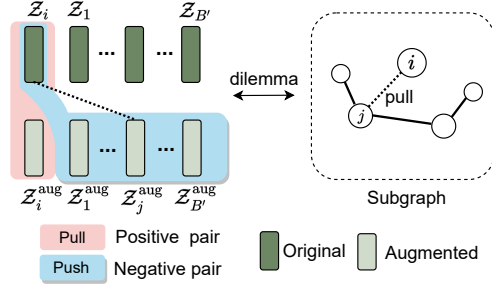


Figure 4: Contrastive samples with negative sample dilemma.

the other samples within the mini-batch are treated as negative pairs, i.e., $\{(X'_i, X'_j)^{\text{aug}}\}_{j=1, j \neq i}^{B'}$. A projection layer maps the spatio-temporal features of the original \mathcal{H} and augmented samples \mathcal{H}^{aug} into latent space \mathcal{Z} and \mathcal{Z}^{aug} , respectively. The contrastive loss \mathcal{L}_{cl} for sample X'_i is then formulated as:

$$\mathcal{L}_{\text{cl}}(X'_i) = -\log \frac{\exp(s_{i,i}/\tau)}{\sum_{j=1}^{B'} \exp(s_{i,j}/\tau)}, \quad (4)$$

where $s_{i,j} = \text{sim}(\mathcal{Z}_i, \mathcal{Z}_j^{\text{aug}})$ denotes the dot-product similarity measuring the feature similarity, and τ is the temperature factor that controls the magnitude of penalties on hard negative samples [30].

3.3.2 Negative Pair Filter. However, vanilla spatio-temporal contrastive learning introduces a unique dilemma regarding the treatment of negative sample pairs. Specifically, as shown in Figure 4 left, a sample X'_i has its negative pair counterpart X'_j^{aug} , where $j \neq i$. The learning process aims to push these samples apart, that is to make them dissimilar. However, a complication arises when X'_i and X'_j belong to the same subgraph \mathcal{G}_i and are connected by an edge (Figure 4 right). In this case, \mathcal{Z}_i and $\mathcal{Z}_j^{\text{aug}}$ should exhibit similar behaviours and thus should be pulled closer together during learning. Experimentally, our ablation study supports this claim, where the performance decreases when vanilla contrastive learning is directly applied (refer to results in Figure 5).

In light of this, we propose to include a negative pair filter into vanilla contrastive learning that adaptively excludes negative sample pairs belonging to the same subgraph. Consequently, Equation (4) is re-formulated as:

$$\mathcal{L}_{\text{cl}}(X'_i) = -\log \frac{\exp(s_{i,i}/\tau)}{\sum_{j=1, j \notin \mathcal{G}_i}^{B'} \exp(s_{i,j}/\tau)}, \quad (5)$$

where \mathcal{G}_i denotes the subgraph containing sample X'_i .

3.3.3 Focal Contrastive Learning (FOCALCL). When constructing negative pairs, we find that imbalanced data would lead to generating hard negative samples, which are excessively similar to positive samples. This makes it challenging for vanilla contrastive learning to learn discriminative representations. To understand this issue formally, consider the following: let $(X'_i, X'_j)^{\text{aug}}$ be a negative pair, and $(X'_i, X'_i)^{\text{aug}}$ be a positive pair, where X'_i is an expanding variable sample and X'_j^{aug} is an augmented sample of a continual variable. When the STEF is optimized with imbalanced data, it would focus on continual variables, overshadowing the distinct patterns of expanding variables. This results in an increase in the similarity

between the negative pair embeddings $(\mathcal{Z}_i^{\text{aug}}, \mathcal{Z}_j^{\text{aug}})$, which diminishes the contrast between positive pair embeddings $(\mathcal{Z}_i^{\text{aug}}, \mathcal{Z}_i^{\text{aug}})$ and negative pair embeddings $(\mathcal{Z}_i^{\text{aug}}, \mathcal{Z}_j^{\text{aug}})$. Consequently, vanilla contrastive learning becomes less effective.

To alleviate this problem, our approach is to concentrate on the samples of expanding variables to compensate for the lack of optimization due to insufficient data. As pointed out by [30], the temperature τ in Equation (5) can control the penalty strength on the above hard negative samples. To improve the optimization of expanding variables, we further introduce a focal temperature factor. This factor adjusts the temperature τ dynamically, thereby refining the learning process for these critical samples. The focal temperature factor can be formulated as follows:

$$\tau_i = \begin{cases} \alpha * \tau, 0 < \alpha < 1.0, & \text{if } X'_i \text{ is expanding variable,} \\ \tau & \text{others.} \end{cases} \quad (6)$$

3.3.4 Joint Objective Loss. Finally, the output layer employs 1×1 convolutions to map the spatio-temporal features \mathcal{H} to the desired Q forecasting timesteps. The overall loss function integrates the focal contrastive loss (using Equation (6) as the temperature τ in Equation (5)) with the mean absolute forecasting error loss. Formally, the joint loss is defined as:

$$\mathcal{L} = \frac{1}{B'} \sum_{i=1}^{B'} \left(-\log \frac{\exp(s_{i,i}/\tau_i)}{\sum_{j=1, j \notin \mathcal{G}_i}^{B'} \exp(s_{i,j}/\tau_i)} + |\hat{Y}_i - Y_i| \right). \quad (7)$$

where $Y = (\mathcal{Y}_1, \dots, \mathcal{Y}_{B'})$ represents the ground truths.

4 EXPERIMENTS

In this section, we comprehensively evaluate the proposed STEV model to investigate its forecasting performance, robustness to various expanding scenarios, and sensitivity to key parameters. Specifically, our experiments aim to answer the following research questions:

- *RQ1:* How does STEV perform on real-world EVTS datasets compared to SOTA methods tailored to EVTTSF? (see Section 4.2)
- *RQ2:* What is the impact of each component of STEV on its performance? (see Section 4.3)
- *RQ3:* Does STEV have an advantage over other methods for addressing data imbalance, such as oversampling and augmentation? (see Section 4.3)
- *RQ4:* How does STEV perform under different variable expanding scenarios? (see Section 4.4)

Table 1: Statistics of evaluation datasets. Notation @ denotes different periods. The data split is train1/train2/valid/test.

Dataset	Sample Rate	# Variables@ P_1	# Variables@ P_2	Data Split
EElectricity	1 hour	261	261+60	925d/7d/3d/321d
EPeMS	5 minutes	296	296+151	63d/3d/2d/22d
EWeather	1 hour	310	310+100	560d/7d/3d/159d

4.1 Experimental setup

4.1.1 Datasets. We used three real-world datasets across different domains for experiments: Electricity [34], PeMS [15], Weather [21]. As these datasets originally had full observations for all variables, we customized them to adapt to EVTTSF. Table 1 shows each dataset's

Table 2: Overall EVTSTF performance comparison between STEV and potential SOTA solutions. The bold values indicate the best performance in the Oracle setting i.e., assuming complete data is available. The bold and value formats indicate the best and suboptimal performance, respectively. The ‘-’ denotes None, where TrafficStream is infeasible on the EElectricity and EWeather datasets due to the lack of a pre-defined graph.

Training Strategy	Dataset Model	Metric	EElectricity				EPeMS				EWeather				
			Continual	Expanding	Overall	Δ	Continual	Expanding	Overall	Δ	Continual	Expanding	Overall	Δ	
Oracle	AGCRN	MAE	0.245	0.200	0.237	-	21.97	22.76	22.23	-	0.723	0.975	0.785	-	
		RMSE	0.386	0.316	0.347	-	35.40	35.03	35.28	-	1.197	1.558	1.294	-	
	GWNENET	MAE	0.281	0.235	0.273	-	22.67	23.55	22.97	-	0.700	0.948	0.760	-	
		RMSE	0.429	0.357	0.414	-	34.60	35.09	34.77	-	1.199	1.590	1.305	-	
	MSGNET	MAE	0.338	0.339	0.338	-	25.26	26.46	25.67	-	0.961	1.321	1.049	-	
		RMSE	0.485	0.468	0.482	-	39.02	39.47	39.17	-	1.559	2.096	1.705	-	
	iTransformer	MAE	0.374	0.345	0.369	-	25.35	25.48	25.39	-	0.830	1.102	0.896	-	
		RMSE	0.581	0.541	0.574	-	40.48	40.42	40.46	-	1.450	1.868	1.562	-	
UTSF	Nbeats	MAE	0.402	0.476	0.407	71.73%	26.91	27.33	27.05	21.68%	0.807	1.596	1.026	35.05%	
		RMSE	0.620	0.856	0.641	84.73%	42.6	41.04	42.08	21.02%	1.416	2.580	1.816	40.37%	
	PatchTST	MAE	0.538	0.507	0.532	124.47%	32.48	33.63	32.87	47.86%	0.919	1.186	0.984	29.86%	
		RMSE	0.799	0.855	0.809	133.14%	50.55	50.10	50.40	45.92%	1.595	1.988	1.699	32.22%	
	GPT4TS	MAE	0.544	0.509	0.537	126.58%	32.02	33.26	32.44	42.07%	0.920	1.194	0.987	29.47%	
		RMSE	0.804	0.840	0.811	133.71%	49.38	49.45	49.40	44.95%	1.600	2.017	1.711	31.29%	
	GRU	MAE	0.407	0.617	0.424	78.90%	27.41	27.9	27.58	24.07%	0.811	5.765	2.188	187.95%	
		RMSE	0.620	1.319	0.700	101.73%	42.93	41.37	42.41	21.97%	1.414	9.830	5.321	311.20%	
	FPTM	AGCRN	MAE	0.248	0.643	<u>0.322</u>	<u>35.86%</u>	<u>23.09</u>	26.86	<u>24.37</u>	<u>9.63%</u>	0.718	1.269	0.852	12.11%
			RMSE	0.388	1.438	0.712	51.26%	36.37	40.32	37.75	8.57%	1.220	2.122	1.491	15.22%
		GWNENET	MAE	0.307	0.526	0.348	46.84%	23.87	<u>25.94</u>	24.57	10.53%	0.750	<u>1.160</u>	<u>0.850</u>	<u>11.84%</u>
			RMSE	0.458	1.059	0.617	77.81%	<u>36.01</u>	<u>38.41</u>	<u>36.84</u>	<u>5.95%</u>	1.284	<u>1.940</u>	<u>1.471</u>	<u>13.68%</u>
MSGNET		MAE	0.35	<u>0.376</u>	0.355	49.79%	26.46	31.79	28.26	27.13%	0.983	1.479	1.104	45.26%	
		RMSE	0.505	<u>0.625</u>	<u>0.530</u>	52.74%	39.25	44.9	41.25	18.64%	1.591	2.308	1.793	38.56%	
iTransformer		MAE	0.382	0.413	0.388	63.71%	26.05	26.5	26.2	17.86%	0.830	1.172	0.896	17.89%	
		RMSE	0.587	0.734	0.617	77.81%	41.15	41.47	41.26	18.67%	1.450	1.991	1.562	20.71%	
Continual Learning	TrafficStream	MAE	-	-	-	-	27.66	27.05	27.45	23.48%	-	-	-	-	
		RMSE	-	-	-	-	40.93	39.37	40.41	16.22%	-	-	-	-	
STEV (ours)		MAE	<u>0.266</u>	0.338	0.280	18.14%	21.93	23.75	22.55	1.44%	<u>0.727</u>	1.067	0.810	6.58%	
		RMSE	<u>0.401</u>	0.611	0.447	29.08%	33.78	35.66	34.42	-1.01%	<u>1.239</u>	1.776	1.389	7.34%	

statistics and data splits. For all datasets, both H and Q are set to 12. The details are as follows: **(i) EElectricity**: This dataset records hourly electricity consumption in kWh of 321 clients from 2012 to 2014. We randomly selected 261 clients as the continual variables over the pre-expanding period (P_1), and the remaining 60 clients as the expanding variables over the post-expanding period (P_2). **(ii) EPeMS**: The PeMS dataset consists of traffic flow data in District 7 of California. Since the sensor location is available, we first selected a central sensor as an anchor and then filtered 296 sensors as the continual variables, with the remaining 151 sensors as expanding variables, based on the spatial distance from the anchor. **(iii) EWeather**: Provided by WeatherBench, this dataset contains 410 nodes on the Earth sphere. We randomly selected 310 nodes as continual variables, and the remaining as expanding variables. In real-world applications, the expansion process varies across different contexts and requirements. Thus, We also tailored the datasets accordingly and explored various expanding scenarios (see Section 4.4). More details can be found in Appendix A.2.

4.1.2 Baselines. We investigated and implemented a series of existing methods that can be tailored for EVTSTF, classifying them into three types: **(1) UTS Forecasting (UTSF)**: these methods forecast EVTS as individual UTS, naturally avoiding the inconsistent shape issue; **(2) First-padding-then-masking MTSF (FPTM)**:

these methods first standardize data shapes through padding and then use SOTA MTSF models with a masking matrix to filter out padding loss; **(3) Continual learning-based MTSF**: these methods train a model from scratch with train1 data (P_1) and then incrementally learn using train2 data (P_2). For each type, we selected widely used models, including GRU [6], N-beats [20], PatchTST [19], and GPT4TS [42]; GWNENET [35], AGCRN [1], MSGNET [2], and iTransformer [16]; and TrafficStream [4].

Besides, we conducted an **Oracle** setting, assuming the availability of P_1 data for expanding variables, allowing each model to be optimized with fully observed data. While impractical, this setting helps verify the *upper bound* for baselines benefiting from full observations. Further experimental implementations are given in Appendix A.4.

4.1.3 Evaluation metrics. We evaluate forecasting performance using Mean Absolute Error (MAE) and Root Mean Square Error (RMSE) averaged over the forecasting horizon. Additionally, we propose to evaluate the performance gap to the *upper bound* by quantifying the performance relative to the Oracle as

$$\Delta = \frac{E_{Expanding} - E_{Oracle}}{E_{Oracle}}. \quad (8)$$

4.2 Overall Results

Table 2 reports the overall performance of different methods on three datasets, including the averaged MAE and RMSE on continual, expanding, and overall variables over 12 timesteps (RQ1). Note that TrafficStream relies on a pre-defined graph to transfer learned information from continual to expanding variables, therefore, we only report the performance on the EPeMS dataset. We observe the following findings: (1) STEV achieves SOTA performance across almost all settings, showing significant average improvements with average reductions of 10.72% in MAE and 11.85% in RMSE compared to the runner-up. This success is primarily attributed to the innovative spatio-temporal focal learning, which effectively focuses on expanding variables. However, STEV does not show improvements for the continual variables in the electricity and weather datasets. This may be due to the coarse-grained temporal modeling with CNNs, akin to the observed performance differences between GWNET and AGCRN. (2) Due to the scarcity of data, the performance of expanding variables declines significantly across all methods. While the GPT4TS and PatchTST separately benefit from the pre-trained large model and weight-sharing mechanism for few-shot learning, they lack explicit spatio-temporal patterns, leading to inferior performance. In contrast, STEV, using only 5% of the complete data (3-day EPeMS data), surpasses methods trained with the Oracle setting, demonstrating its ability to effectively learn representations for expanding variables. (3) Although the FPTM-based strategy introduces padding values, it captures spatio-temporal correlations more effectively than the solely temporal modeling used in UTSF-based strategies, leading to better overall performance. (4) The continual learning approach benefits from leveraging a pre-trained model and incrementally learning from new observations during the expansion period. However, this can lead to catastrophic forgetting, which negatively affects the model’s performance on both continual and expanding variables.

4.3 Ablation Study

We perform an ablation study on the EPeMS data to verify the effectiveness of each component of STEV (RQ2). We review four components of STEV, including (1) *FLATS* which allows STEV to learn spatio-temporal dependencies under varying variables; (2) *Contrastive Learning* (CL) which enhances STEV to learn robust representations for both continual and expanding variables; (3) *Negative Filter* (NF) which allows STEV to exclude inappropriate negative pairs in contrastive learning; (4) *FOCALCL* which enables STEV to focus on expanding variables and thus alleviate the impact of imbalanced data.

We gradually add each of the above modules starting from FLATS. Note that when FOCALCL is added, it forms STEV. From Fig. 5 we observe a continuous performance improvement, except for the variant w/ CL. As discussed in Section 3.3.2, there is a dilemma between the naive CL and spatial module. We thus propose the negative filter to remove conflict negative samples.

We additionally compared two conventional solutions for data imbalance (RQ3), i.e., oversampling (OS) and data augmentation (DA). In our experiments, the double sampling rate and the mixup augmentation technique [39] are utilized on the expanding data. Table 3 shows that the performance is comparable with data-level

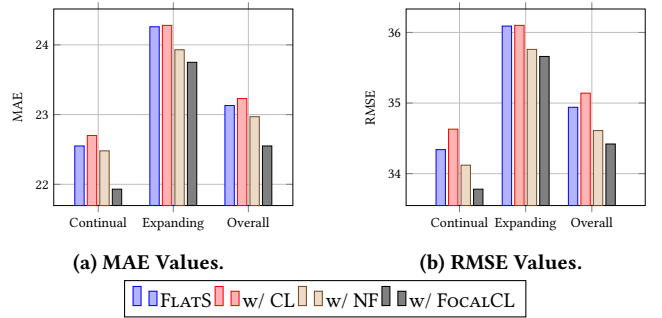


Figure 5: Ablation Study of STEV in terms of MAE and RMSE. techniques, and using oversampling even leads to a decrease. To explore the effect of the ultra data augmentation, we conduct the DA^* experiment, augmenting the entire dataset. Despite the improved performance, the computational overhead doubled.

Table 3: Comparison of various conventional solutions for the imbalanced issue on EPeMs.

Variants	Continual		Expanding		Overall	
	MAE	RMSE	MAE	RMSE	MAE	RMSE
STEV	21.93	33.78	23.75	35.66	22.55	34.42
FLATS	22.55	34.34	24.26	36.09	23.13	34.94
FLATS w/ OS	22.88	34.41	24.49	36.06	23.42	34.98
FLATS w/ DA	22.43	34.19	24.36	36.02	23.16	34.83
FLATS w/ DA^*	22.19	33.95	24.11	36.09	22.84	34.69

Table 4: Consecutive expansion setting

#Var@P1	#Var@P2	#Var@P3	#days@train1	@train2	@train3
296	427	447	59	4	3

Table 5: Performance on the consecutive Expansion.

Model		Con@P1	Exp@P2	Exp@P3	Overall
		MAE	22.40	23.21	23.78
STEV	RMSE	34.19	34.79	37.94	34.49
	MAE	23.25	24.11	25.55	23.62
FPTM-GWNET	RMSE	35.25	35.93	38.55	35.64

4.4 Expanding Scenario Exploration

To explore the generalizability of STEV in real-world scenarios, we conduct comprehensive experiments on the EPeMS dataset under various expansion settings, involving the partition of continual and expanding variables, the number of expansions, and the duration of the expansion period (RQ4).

We first simulate three potential demands of expanding variables in the traffic domain, including (1) Area-based expansions where new sensors are deployed in specific focus areas, with those in the top-left region remaining as continual variables (see Fig. 6a); (2) Spatial-based expansions where sensors spread to the surrounding areas with the expansion of urban monitor planning. A central sensor and 296 sensors within a 30 km radius serve as continual variables, while others are expanding variables (see Fig. 6b); and (3) Internal expansions where the denser sensor network increases perception density. We randomly select 296 sensors as continual

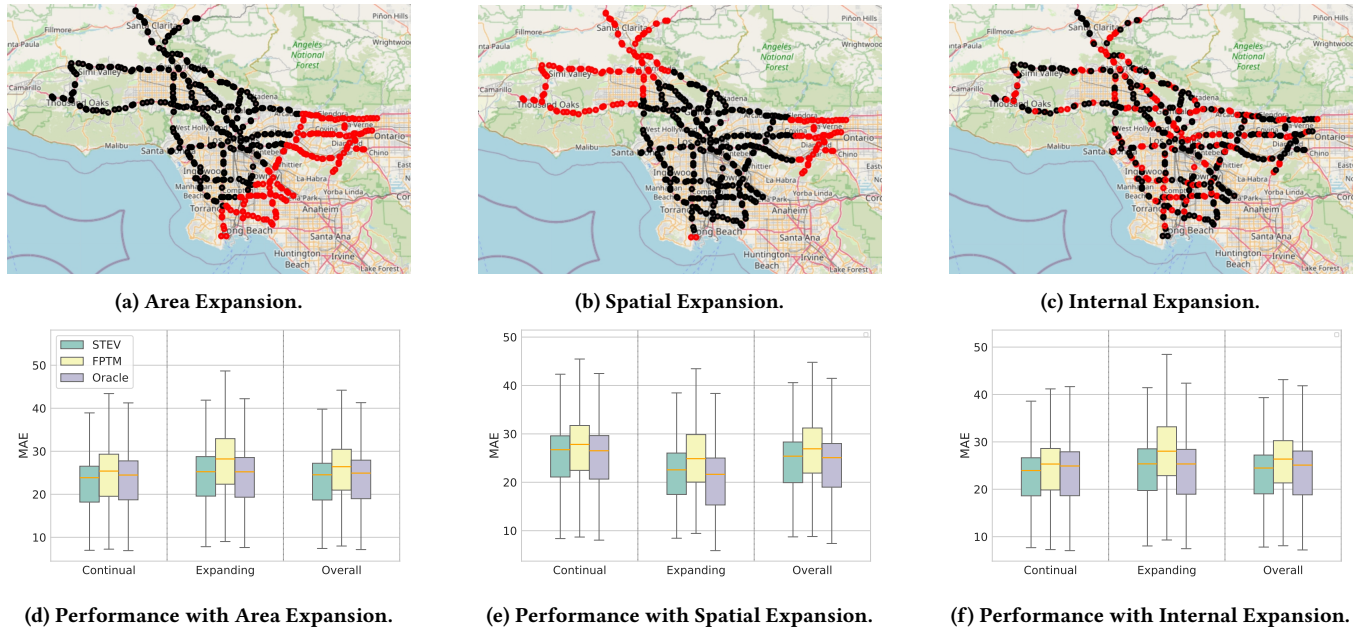


Figure 6: Visualization of geographic distribution (a)-(c) and performance comparison with three expanding scenarios (d)-(f). In (a)-(c), black nodes represent continual variables, and red nodes indicate expanding variables.

Table 6: Performance on a longer observation period.

Model		Continual(52d)	Expanding(14d)	Overall
STEV	MAE	22.17	23.05	22.47
	rmse	33.95	34.52	34.15
FPTM-GWNET	MAE	22.70	24.62	23.35
	RMSE	34.67	36.69	35.37

variables (see Fig. 6c). As shown in Fig. 6, STEV consistently outperforms FPTM-GWNET [35] across all three scenarios, demonstrating strong generalization capability.

To assess the adaptability, we conduct a consecutive experiment involving two-time spatial expansions. Table 4 details the variable statistics and durations, while Table 5 reports performance results. The findings show that STEV consistently outperforms FPTM-GWNET across all metrics, for both continual and expanding variables, confirming its robustness in handling dynamic spatial expansions.

We further examine STEV’s performance over the much longer period of sensor deployment, by conducting experiments on the expanding period over 14 days. Table 6 shows that STEV maintains superiority over FPTM-GWNET, even as data scarcity diminishes over time. Compared to the 3-day results (Table 2), STEV effectively captures evolving spatiotemporal patterns, demonstrating its stability across both short- and long-term deployments.

5 RELATED WORK

Multivariate Time Series Forecasting. Extensive deep learning-based MTSF methods prove that both capturing intra-series temporal dependencies and inter-series spatial dependencies are beneficial for modeling future changes [16, 23, 36, 40]. Particularly, spatio-temporal graph neural networks such as Graph WaveNet [35] and AGCRN [1] further enhance spatio-temporal representations by

combining GNNs with LSTM and GNNs with TCN, respectively. However, these works cannot be directly performed in the EVTSF task. Even with padding strategies, their performance still suffers from data imbalance. Recent efforts [4, 29] have explored the expansion of traffic networks where observed traffic areas are continuously expanding as new sensors are deployed. These studies primarily address this problem as a two-phase learning task within the continual learning or online learning paradigm [5]. The main challenge that these studies intend to address, is the catastrophic forgetting phenomenon [10]. They first discover the continual variables that need to learn new patterns, then employ historical data replay [22], elastic weight consolidation [12], and memory bank mechanism [17] to consolidate historical knowledge. In contrast, the performance achieved by the retraining paradigm is an upper bound of continual learning due to the global optimization for model parameters with better convergence and performance [12, 22]. Another similar task to EVTSF is spatio-temporal Kriging [33], a.k.a. spatio-temporal extrapolation [11], which performs imputation for expanding variables based on the context of continual variables. Although both are aimed at expanding variables, it has different learning objectives from EVTSF.

Contrastive Learning in Time Series. Recently, unsupervised contrastive learning has gained significant traction in the time series domain [14, 26, 38]. The primary objective of this approach is to make positive samples attractive and separate negative samples, thereby enabling the learning of inherent temporal characteristics. Prior efforts mainly explore the effect of positive and negative pairs. For instance, motivated by the local smoothness of a signal during the generative process, TNC [26] encourages the consistency of samples within a temporal neighborhood. TS2Vec [38] learns contextual information between timesteps at different temporal resolutions. In this approach, two augmented views of the same

time step exhibit similarity and are considered dissimilar otherwise. To further explore the impact of augmentation, TimesURL [14] employs a frequency-temporal-based augmentation technique to encourage temporal consistency. However, due to the imbalanced data and the potential conflict between negative samples in contrastive learning and neighbors in the graph structure, directly leveraging contrastive learning is hard to benefit EVTSF (refer to Table 3).

6 CONCLUSION

In this paper, we introduced a new task called Expanding Multivariate Time Series Forecasting (EVTSF), driven by the practical needs of sensing expansion in Cyber-Physical Systems. To tackle this, we propose STEV, a flexible spatio-temporal forecasting framework to address two key challenges: inconsistent data shape and imbalanced spatio-temporal learning. Specifically, our approach features a Flat Scheme that unifies data shapes with a simple flattening operation, making the model agnostic to variable scale. Besides, we employed Focal Contrastive Learning to enhance the learning of robust and discriminative spatio-temporal feature representations, with a focal contrastive loss that emphasizes optimizing expanding variables. We conducted extensive experiments on three real-world datasets, demonstrating that STEV significantly enhances performance on variables with limited observations and achieves results comparable to, or better than, methods using complete data. Furthermore, an intriguing avenue for future research could involve exploring the out-of-distribution problem, particularly how data distribution shifts after the deployment of new sensors.

REFERENCES

- [1] Lei Bai, Lina Yao, Can Li, Xianzhi Wang, and Can Wang. 2020. Adaptive graph convolutional recurrent network for traffic forecasting. In *Advances in Neural Information Processing Systems*, Vol. 33. 17804–17815.
- [2] Wanlin Cai, Yuxuan Liang, Xianggen Liu, Jianshuai Feng, and Yuankai Wu. 2024. MSGNet: Learning Multi-Scale Inter-series Correlations for Multivariate Time Series Forecasting. In *AAAI Conference on Artificial Intelligence*. 11141–11149.
- [3] Ting Chen, Simon Kornblith, Mohammad Norouzi, and Geoffrey Hinton. 2020. A simple framework for contrastive learning of visual representations. In *International Conference on Machine Learning*. 1597–1607.
- [4] Xu Chen, Junshan Wang, and Kunqing Xie. 2021. TrafficStream: A streaming traffic flow forecasting framework based on graph neural networks and continual learning. In *AAAI Conference on Artificial Intelligence*.
- [5] Zhiyuan Chen and Bing Liu. 2018. *Lifelong machine learning*. Vol. 1. Springer.
- [6] Junyoung Chung, Caglar Gulcehre, KyungHyun Cho, and Yoshua Bengio. 2014. Empirical evaluation of gated recurrent neural networks on sequence modeling. *arXiv preprint arXiv:1412.3555* (2014).
- [7] Michaël Defferrard, Xavier Bresson, and Pierre Vandergheynst. 2016. Convolutional neural networks on graphs with fast localized spectral filtering. In *Advances in Neural Information Processing Systems*, Vol. 29.
- [8] Bingbing Dong, Xingliang Jiang, and Fanghui Yin. 2022. Development and prospect of monitoring and prevention methods of icing disaster in China power grid. *IET Generation, Transmission & Distribution* 16, 22 (2022), 4480–4493.
- [9] Matthias Fey and Jan Eric Lenssen. 2019. Fast graph representation learning with PyTorch Geometric. In *ICLR Workshop on Representation Learning on Graphs and Manifolds*.
- [10] Robert M French. 1999. Catastrophic forgetting in connectionist networks. *Trends in cognitive sciences* 3, 4 (1999), 128–135.
- [11] Junfeng Hu, Yuxuan Liang, Zhencheng Fan, Hongyang Chen, Yu Zheng, and Roger Zimmermann. 2023. Graph Neural Processes for Spatio-Temporal Extrapolation. In *ACM SIGKDD Conference on Knowledge Discovery and Data Mining*. 752–763.
- [12] James Kirkpatrick, Razvan Pascanu, Neil Rabinowitz, Joel Veness, Guillaume Desjardins, Andrei A Rusu, Kieran Milan, John Quan, Tiago Ramalho, Agnieszka Grabska-Barwinska, et al. 2017. Overcoming catastrophic forgetting in neural networks. *National Academy of Sciences* 114, 13 (2017), 3521–3526.
- [13] Yaguang Li, Rose Yu, Cyrus Shahabi, and Yan Liu. 2018. Diffusion Convolutional Recurrent Neural Network: Data-Driven Traffic Forecasting. In *6th International Conference on Learning Representations*.
- [14] Jiexi Liu and Songcan Chen. 2024. TimesURL: Self-supervised contrastive learning for universal time series representation learning. In *AAAI Conference on Artificial Intelligence*, Vol. 38. 13918–13926.
- [15] Xu Liu, Yutong Xia, Yuxuan Liang, Junfeng Hu, Yiwei Wang, Lei Bai, Chao Huang, Zhengguang Liu, Bryan Hooi, and Roger Zimmermann. 2024. LargeST: A benchmark dataset for large-scale traffic forecasting. *Advances in Neural Information Processing Systems* 36 (2024).
- [16] Yong Liu, Tengge Hu, Haoran Zhang, Haixu Wu, Shiyu Wang, Lintao Ma, and Mingsheng Long. 2023. iTransformer: Inverted transformers are effective for time series forecasting. *arXiv preprint arXiv:2310.06625* (2023).
- [17] David Lopez-Paz and Marc’Aurelio Ranzato. 2017. Gradient episodic memory for continual learning. In *Advances in Neural Information Processing Systems*, Vol. 30.
- [18] Minbo Ma, Jilin Hu, Christian S. Jensen, Fei Teng, Peng Han, Zhiqiang Xu, and Tianrui Li. 2024. Learning Time-Aware Graph Structures for Spatially Correlated Time Series Forecasting. In *International Conference on Data Engineering*. 4435–4448.
- [19] Yuqi Nie, Nam H. Nguyen, Phanwadee Sinthong, and Jayant Kalagnanam. 2023. A Time Series is Worth 64 Words: Long-term Forecasting with Transformers. In *International Conference on Learning Representations*.
- [20] Boris N. Oreshkin, Dmitri Carpov, Nicolas Chapados, and Yoshua Bengio. 2020. N-BEATS: Neural basis expansion analysis for interpretable time series forecasting. In *International Conference on Learning Representations*.
- [21] Stephan Rasp, Peter D Dueben, Sebastian Scher, Jonathan A Weyn, Soukayna Mouatadid, and Nils Thuerey. 2020. WeatherBench: a benchmark data set for data-driven weather forecasting. *Journal of Advances in Modeling Earth Systems* 12, 11 (2020).
- [22] David Rolnick, Arun Ahuja, Jonathan Schwarz, Timothy Lillicrap, and Gregory Wayne. 2019. Experience replay for continual learning. *Advances in neural information processing systems* 32 (2019).
- [23] Xingjian Shi, Zhourong Chen, Hao Wang, Dit-Yan Yeung, Wai-Kin Wong, and Wang-chun Woo. 2015. Convolutional LSTM Network: A machine learning approach for precipitation nowcasting. *Advances in neural information processing systems* 28 (2015).
- [24] Stephen A Shield, Steven M Quiring, Jordan V Pino, and Ken Buckstaff. 2021. Major impacts of weather events on the electrical power delivery system in the United States. *Energy* 218 (2021), 119434.
- [25] Mingtian Tan, Mike A Merrill, Vinayak Gupta, Tim Althoff, and Thomas Hartvigsen. 2024. Are language models actually useful for time series forecasting?. In *The Thirty-eighth Annual Conference on Neural Information Processing Systems*.
- [26] Sana Tonekaboni, Danny Eytan, and Anna Goldenberg. 2021. Unsupervised representation learning for time series with temporal neighborhood coding. In *International Conference on Learning Representations*.
- [27] G. M. Van de Ven, T. Tuytelaars, and A. S. Tolias. 2022. Three types of incremental learning. *Nature Machine Intelligence* 4 (2022), 1185–1197.
- [28] Aäron van den Oord, Sander Dieleman, Heiga Zen, Karen Simonyan, Oriol Vinyals, Alex Graves, Nal Kalchbrenner, Andrew W. Senior, and Koray Kavukcuoglu. 2016. WaveNet: A Generative Model for Raw Audio. In *The 9th ISCA Speech Synthesis Workshop*. 125.
- [29] Binwu Wang, Yudong Zhang, Xu Wang, Pengkun Wang, Zhengyang Zhou, Lei Bai, and Yang Wang. 2023. Pattern expansion and consolidation on evolving graphs for continual traffic prediction. In *ACM SIGKDD Conference on Knowledge Discovery and Data Mining*. 2223–2232.
- [30] Feng Wang and Huaping Liu. 2021. Understanding the behaviour of contrastive loss. In *IEEE/CVF conference on Computer Vision and Pattern Recognition*. 2495–2504.
- [31] Yihe Wang, Yu Han, Haishuai Wang, and Xiang Zhang. 2023. Contrast Everything: A Hierarchical Contrastive Framework for Medical Time-Series. In *Advances in Neural Information Processing Systems*, Vol. 36. 55694–55717.
- [32] Junkang Wu, Jiawei Chen, Jiancan Wu, Wentao Shi, Xiang Wang, and Xiangnan He. 2023. Understanding Contrastive Learning via Distributionally Robust Optimization. In *Advances in Neural Information Processing Systems*, Vol. 36. Curran Associates, Inc., 23297–23320.
- [33] Yuankai Wu, Dingyi Zhuang, Aurelie Labbe, and Lijun Sun. 2021. Inductive graph neural networks for spatiotemporal kriging. In *AAAI Conference on Artificial Intelligence*. 4478–4485.
- [34] Zonghan Wu, Shirui Pan, Guodong Long, Jing Jiang, Xiaojun Chang, and Chengqi Zhang. 2020. Connecting the dots: Multivariate time series forecasting with graph neural networks. In *ACM SIGKDD international conference on Knowledge Discovery and Data Mining*. 753–763.
- [35] Zonghan Wu, Shirui Pan, Guodong Long, Jing Jiang, and Chengqi Zhang. 2019. Graph wavenet for deep spatial-temporal graph modeling. In *International Joint Conferences on Artificial Intelligence*.
- [36] Kun Yi, Qi Zhang, Wei Fan, Hui He, Liang Hu, Pengyang Wang, Ning An, Longbing Cao, and Zhendong Niu. 2023. FourierGNN: Rethinking Multivariate Time Series Forecasting from a Pure Graph Perspective. In *Advances in Neural Information Processing Systems*, Vol. 36. 69638–69660.

- [37] Fisher Yu and Vladlen Koltun. 2016. Multi-Scale Context Aggregation by Dilated Convolutions. In *International Conference on Learning Representations*.
- [38] Zhihan Yue, Yujing Wang, Juanyong Duan, Tianmeng Yang, Congrui Huang, Yunhai Tong, and Bixiong Xu. 2022. TS2Vec: Towards universal representation of time series. In *AAAI Conference on Artificial Intelligence*, Vol. 36. 8980–8987.
- [39] Hongyi Zhang, Moustapha Cissé, Yann N. Dauphin, and David Lopez-Paz. 2018. mixup: Beyond Empirical Risk Minimization. In *6th International Conference on Learning Representations*.
- [40] Junbo Zhang, Yu Zheng, and Dekang Qi. 2017. Deep spatio-temporal residual networks for citywide crowd flows prediction. In *AAAI conference on Artificial Intelligence*, Vol. 31.
- [41] Yu Zheng, Furu Li, and Hsun-Ping Hsieh. 2013. U-air: When urban air quality inference meets big data. In *ACM SIGKDD international conference on Knowledge Discovery and Data mining*. 1436–1444.
- [42] Tian Zhou, Peisong Niu, Xue Wang, Liang Sun, and Jin Rong. 2023. One Fits All: Power General Time Series Analysis by Pretrained LM. In *NeurIPS*.

A APPENDIX: REPRODUCIBILITY

This section outlines the details of STEV implementation to ensure reproducibility.

A.1 Details of Spatio-temporal Feature Extractor

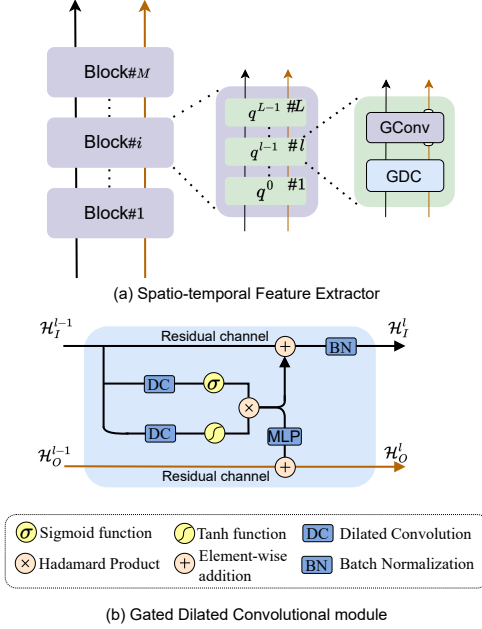


Figure 7: The architecture of Spatio-temporal Feature Extractor.

To efficiently capture multi-scale temporal dependencies and spatial dependencies, following [34], the spatio-temporal feature extractor employs a deep residual architecture that incorporates Gated Dilated Convolutional module (GDC) with 1D dilated convolution [37] and Graph Convolutional module (GConv) with chebyshev spectral graph convolution [7]. As depicted in Figure 7 (a), the basic block contains a multi-layer spatio-temporal convolutional architecture with various receptive fields. For the sake of simplicity, we focus on describing the operation of the l -th layer of the i -th block in detail. Given the hidden features \mathcal{H}_I^{l-1} , and \mathcal{H}_O^{l-1} , representing the inner and outer residual connections, and $\mathcal{H}_I^0 = \text{Embed}(X)$, $\mathcal{H}_O^0 = \mathbf{0}$, then the two outputs of l -th layer features can be formulated as,

$$\mathcal{U} = \tanh(\mathcal{H}_I^{(l-1)} \star f_{1 \times k}^d) \odot \sigma(\mathcal{H}_I^{(l-1)} \star f_{1 \times k}^d) \quad (9)$$

$$\mathcal{H}_I^{(l)} = \text{BatchNorm}(\mathcal{H}_I^{(l-1)} + \mathcal{U}) \quad (10)$$

$$\mathcal{H}_O^{(l)} = \text{MLP}(\mathcal{H}_O^{(l-1)}) + \mathcal{U} \quad (11)$$

$$\mathcal{H}_I^{(l)} = \sum_{j=1}^J \mathbf{C}^{(j)} \cdot \Theta^{(j)} \quad (12)$$

where $\mathcal{H} \star f_{1 \times k}$ denotes dilated convolution [28] with kernel size k and dilated factor $d = q^{l-1}$ and q is an increased rate; for spectral graph convolution, $\mathbf{C}^{(1)} = \mathcal{H}_I^{(l)}$, $\mathbf{C}^{(2)} = \hat{\mathbf{L}}\mathcal{H}_I^{(l)}$, $\mathbf{C}^{(j)} = 2 \cdot \hat{\mathbf{L}}\mathbf{C}^{(j-1)} - \mathbf{C}^{(j-2)}$, $\hat{\mathbf{L}}$ represents the symmetric normalization $\mathbf{L} = \mathbf{I} - \mathbf{D}^{-1/2}\mathbf{A}\mathbf{D}^{-1/2}$, \mathbf{D} is the degree matrix, and $\Theta \in \mathbb{R}^{C_{in} \times C_{out}}$ is a parameter matrix.

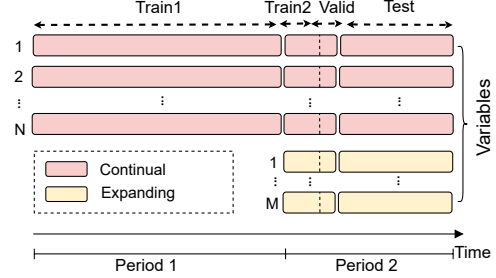


Figure 8: Illustration of Data Partition.

A.2 Data

We craft three real-world datasets across different domains for the EVTFS experiments, including Electricity [34], PeMS [15], and WeatherBench [21], due to the lack of public-availability EVTS data. Originally, these data have complete observations for all variables, we therefore customer them to adapt to the EVTFS task. Fig. 8 visualizes the partition of training, valid, and test sets. Notably, there are two partitions of training data: train1 and train2, representing training data before and after expansion, respectively. For variable partitioning, we first determine quantities based on empirical proportions, then utilize random selection, and spatial center to filter variables depending on whether location is available. As for the duration of data collection for the expanding period, a minimum periodic observation is adopted based on the principle of timely prediction. Table 1 shows the statistics and data splits for each dataset. In real-world applications, the expansion process varies across different contexts and requirements. Thus, we also tailored the datasets accordingly and explored various expanding scenarios (see Section 4.4). The details of each dataset are as follows:

- **EElectricity**: This dataset records hourly electricity consumption in kWh of 321 clients from 2012 to 2014. In this context, expansion refers to the new clients integrated into the grid. Due to the absence of location information and without loss of generality, we randomly selected 261 clients as the continual variables over the pre-expanding period (P_1), and the remaining 60 clients as the expanding variables over the post-expanding period (P_2).
- **EPeMS**: The PeMS dataset involves sensors monitoring traffic flow in District 7 of California, where variables represent sensors. In this context, expansion refers to the installation of new traffic flow sensors at different locations. Since the sensor location is available, we first selected a central sensor as an anchor and then filtered 296 sensors as the continual variables based on the spatial distance from the anchor, with the remaining 151 sensors as expanding variables.

- **EWeather:** The dataset records the temperature from 410 stations on the Earth sphere. Similar to Electricity, We randomly selected 310 stations as continual variables, and the remaining as expanding variables.

Figure 8 further visualizes the partition of training, valid, and test sets. Note that there are two partitions of training data: train1 and train2, representing training data before and after expansion, respectively.

A.3 Baselines

We investigated and implemented a series of existing methods that can be tailored for EVTSTF. They are classified into three types:

- **UTS Forecasting (UTSF):** These methods treat the EVTSTF task as the individual UTS forecasting, naturally avoiding the inconsistent shape issue, including GRU [6], a recurrent neural network variant to capture temporal dependencies by leveraging gating mechanisms; Nbeats [20], a deep neural architecture that combines the backward and forward residual connections, and deep stacked fully connected layers; PatchTST [19], a Transformer with subseries-level patches and channel-independence; and GPT4TS [42], a fine-tuning time series analysis architecture by pre-trained large model.
- **First-padding-then-masking MTSF (FPTM):** We standardize data shape through padding operation and then employ SOTA MTSF models. We also utilize a masking matrix to filter out padding loss to alleviate the data noise impact caused by the filling value. The SOTA methods include GWNET [35], a spatio-temporal graph convolutional network with a self-learning adjacency matrix and stacked dilated 1D convolution to capture spatio-temporal dependencies; AGCRN [1], an adaptive graph convolutional recurrent network that employs graph convolution gated recurrent units to capture interdependencies among variables and intra-variable temporal dependencies; MSGNET [2], a spatio-temporal graph network that learns the inter-series correlations across multiple time scales with frequency domain analysis; and iTransformer [16], a Transformer that captures multivariate correlations via attention mechanism and the feed-forward network on variate tokens.
- **Continual learning-based MTSF:** These methods train a model from scratch with the initial data (P_1) and then incrementally learn using the expanding data (P_2). The TrafficStream [4] is included that consolidates the knowledge learned previously and transfers it to the current model to learn traffic expansion and evolving patterns.

A.4 Experimental Implemets

All methods are conducted with NVIDIA GeForce RTX 3090Ti with PyTorch library. The Adam with a learning rate of $1e-3$ is to optimize parameters. The early stopping is used to confirm the optimal weights in which the training process ends until the performance on the valid set does not improve within 10 patients. For all datasets, the historical observations over 12 time steps are inputted to obtain the predictions over the next 12 time steps, i.e., both H and Q are set to 12. The focal factor α is set to 0.3 for three datasets. Apart from the factor, we follow the hyper-parameters setting with MTGNN [34]. Specifically, the batch size is set to 16. The number of blocks M

is set to 4. The number of layers L is set to 2. The dimensions of node and time embeddings are set to 20 and 10. In the gated dilated convolutional module, the dilated rate q is set to 2, and the kernel size is set to 2. The temporal and spatial convolution modules both have 32 output channels.

A.5 Hyperparameter Study

Table 7: Varying α of focal contrastive loss.

α	Continual		Expanding		Overall	
	MAE	RMSE	MAE	RMSE	MAE	RMSE
0.05	22.10	33.88	23.80	35.72	22.68	34.51
0.1	21.96	33.71	23.59	35.43	22.51	34.30
0.3	21.93	33.78	23.75	35.66	22.55	34.42
0.5	22.13	34.02	23.80	35.60	22.69	34.56
0.7	22.20	33.98	23.86	35.46	22.76	34.49
1.0	22.48	34.12	23.93	35.56	22.97	34.61

The STEV model introduces a novel hyperparameter, the focal weight α , which plays a crucial role in controlling the strength of attention directed toward expanding variables. Table 7 presents the experimental results under various settings of α , highlighting its impact on model performance. Notably, when $\alpha = 1.0$, our loss function aligns with the commonly used contrastive loss, ensuring a balanced treatment of both continual and expanding variables. As α decreases, the optimization process increasingly prioritizes the representation learning of expanding variables, thereby improving their performance. However, this shift comes at a potential cost: excessive emphasis on expanding variables can lead to over-optimization, which may adversely affect the performance of continual variables. These findings emphasize the importance of carefully tuning α to achieve a balanced trade-off between continual and expanding variable modeling, ensuring optimal performance across the dataset.

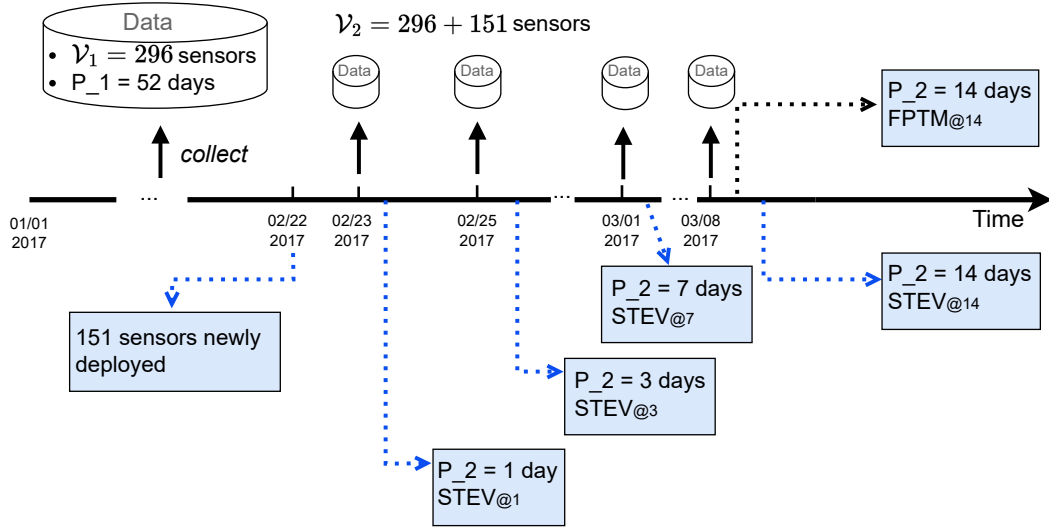
Table 8: Computational and memory analysis

Model	MFLOPs	Parameters(M)
STEV	522.494	0.7252
GWNET	843.049	0.3082
PatchTST	33835.253	6.3472
iTransformer	5652.025	6.3257

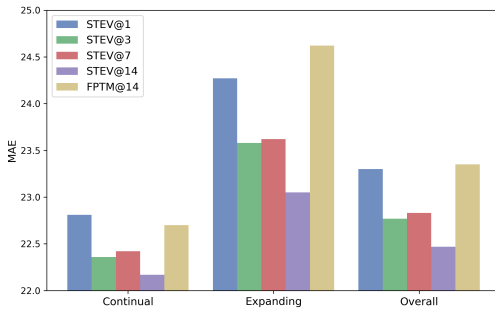
B APPENDIX: EMPIRICAL STUDY

B.1 Efficiency Analysis

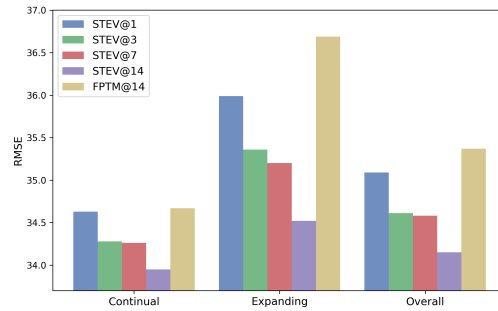
Table 8 provides a comparative analysis of the computational and memory efficiency of the proposed STEV model against several baseline methods, focusing on the number of floating-point operations (MFLOPs) and the total number of model parameters. The results show that STEV strikes a remarkable balance between model size



(a) The traffic flow forecasting model training procedure at various waiting times for data collection. \mathcal{V}_1 and \mathcal{V}_2 denote two variable sets of the before and after expansion. P_1 and P_2 denote two periods before and after expansion.



(b) Performance on MAE.



(c) Performance on RMSE.

Figure 9: Case Study

and computational efficiency, enabling a highly feasible solution for real-world applications.

B.2 Case Study

We further investigate the effectiveness of STEV in timely prediction through a case study. Figure 9a presents the model learning process at various waiting times for data collection. In this study, data for the first period (P_1) were collected over 52 days from 296 sensors, after which 151 additional sensors were deployed to expand the sensing range for traffic flow monitoring in District 7, California. In this context, the forecasting model is keen to be trained after collecting considerable data. To simulate different data collection scenarios, we conducted model training using four distinct durations representing waiting times after the deployment of new sensors: 1 day, 3 days, 7 days, and 14 days. For comparison, we also utilized the runner-up

baseline method, FPTM-GWNET, trained with a total of 66 days of data ($P_1 + P_2 = 52 + 14$). Fig. 9b and Fig. 9c report the forecasting performance on MAE and RMSE.

The results reveal that STEV, even when trained with just 1-day data, outperforms FPTM-GWNET trained on the 14-day data. This demonstrates the strong capability of STEV to quickly adapt to newly added variables and deliver accurate forecasts, meeting the requirements of the proposed expanding-variate time series forecasting task for timely predictions. Furthermore, the performance evaluations across the four durations show that STEV not only effectively learns spatio-temporal dependencies under extreme data imbalance (with only 1 day of data) but also achieves consistent improvements as the volume of augmented variable data increases (up to 14 days). These findings highlight the adaptability of STEV in handling dynamic and evolving spatio-temporal data for real-world timely prediction tasks.